Journal of Power Sources 193 (2009) 454–461

Contents lists available at ScienceDirect

Journal of Power Sources

journal homepage: www.elsevier.com/locate/jpowsour

Air plasma spray processing and electrochemical characterization of Cu–SDC coatings for use in solid oxide fuel cell anodes

Nir Benoved [a], O. Kesler [b,*]

[a] Department of Mechanical Engineering, The University of British Columbia, 2054-6250 Applied Sciences Lane, Vancouver, British Columbia, Canada V6T 1Z4
[b] Department of Mechanical and Industrial Engineering, University of Toronto, 5 King's College Road, Toronto, Ontario, Canada M5S 3G8

ARTICLE INFO

Article history:
Received 13 February 2009
Received in revised form 30 March 2009
Accepted 9 April 2009
Available online 17 April 2009

Keywords:
Solid oxide fuel cells (SOFCs)
Plasma spraying
Cu–SDC based anodes

ABSTRACT

Air plasma spraying has been used to produce porous composite anodes based on $Ce_{0.8}Sm_{0.2}O_{1.9}$ (SDC) and Cu for use in solid oxide fuel cells (SOFCs). Preliminarily, a range of plasma conditions has been examined for the production of composite coatings from pre-mixed SDC and CuO powders. Plasma gas compositions were varied to obtain a range of plasma temperatures. After reduction in H_2, coatings were characterized for composition and microstructure using EDX and SEM. As a result of these tests, symmetrical sintered electrolyte-supported anode–anode cells were fabricated by air plasma spraying of the anodes, followed by in situ reduction of the CuO to Cu. Full cells deposited on SS430 porous substrates were then produced in one integrated process. Fine CuO and SDC powders have been used to produce homogeneously mixed anode coatings with higher surface area microstructures, resulting in area-specific polarization resistances of 4.8 $\Omega\,cm^2$ in impedance tests in hydrogen at 712 °C.

1. Introduction

Fuel cells convert the chemical energy of a fuel, such as hydrogen, into electrical energy very efficiently on many size scales, without combustion and with little or no emission of pollutants. Solid oxide fuel cells (SOFCs) are highly efficient, entirely solid-state fuel cells that operate at high temperatures. They can be used for large-scale central power generation, for distributed generation, or for auxiliary power in transportation. When hydrogen is used to power solid oxide fuel cells, water is the only local emission produced, and the fuel cells experience relatively low degradation rates and fast electrochemical kinetics. However, hydrogen must be generated, compressed, and transported, thus creating high energy requirements and correspondingly higher costs compared to more readily available fuels. Using carbon-containing fuels, such as coal gas, methanol, ethanol, natural gas, gasoline, diesel, carbon monoxide, or renewable bio-fuels to power SOFCs may allow faster commercialization and more widespread use. Widespread power generation from carbon containing fuels using fuel cells rather than combustion engines will result in substantial reductions in greenhouse gas and acid gas emissions due to the absence of nitrogen oxides and the higher efficiency of electrochemical energy conversion.

1.1. SOFC anodes based on Cu–SDC for direct oxidation of hydrocarbon fuels

When using hydrocarbon fuels such as methane, the fuel is typically converted through steam reforming to CO and H_2, which are then consumed electrochemically within the fuel cell, or in the case of CO, reacted with steam to form CO_2 and H_2 through a water gas shift reaction. The reforming reaction can take place externally, in a reformer placed prior to the fuel cell inlet. This configuration, however, increases the overall cost and complexity of the system. Reforming of the fuel in a high temperature SOFC system can also take place within the fuel cell itself, utilizing a reforming catalyst, commonly nickel, in the SOFC anode. This process is known as internal reforming. Internal reforming eliminates the requirement for an external reformer and therefore simplifies the balance of plant system and reduces costs. In addition to reduced costs, internal reforming is endothermic for methane, and therefore it can assist in thermal management of the cell. However, steam reforming of petroleum-based hydrocarbons such as naphtha is less endothermic, and exothermic when the temperature is lowered below 600 °C [1].

Although internal reforming simplifies the SOFC balance of plant, it is still limited in practice due to technological issues. Experiments on internal methane steam reforming have shown that the strong activity of the nickel anode results in a marked temperature reduction in a very localized reaction zone that may lead to steep thermal gradients and thermal stresses [2]. Another disadvantage of steam reforming is that the reforming reaction is endothermic

* Corresponding author. Tel.: +1 416 978 3835; fax: +1 416 978 7753.
E-mail addresses: benoved@interchange.ubc.ca (N. Benoved), kesler@mie.utoronto.ca (O. Kesler).

0378-7753/$ – see front matter © 2009 Elsevier B.V. All rights reserved.
doi:10.1016/j.jpowsour.2009.04.003

and has a high temperature requirement. When the fuel is reformed by steam, high equilibrium conversions require high temperatures. For example, the equilibrium conversion of methane for a H_2O/CH_4 ratio of one at 1 bar is only 37% at 600 °C, 68% at 700 °C, and 87% at 800 °C, and for a H_2O/CH_4 ratio of two at 1 bar is 62% at 600 °C, 77% at 700 °C, and 100% at 800 °C. A higher H_2O/CH_4 ratio increases the extent of reformation of CH_4 to H_2, but it dilutes the fuel and thereby decreases the overall cell efficiency. If reforming is to be performed internally in an SOFC, the high temperature requirement for equilibrium conversion limits the choice of materials that can be used to construct the fuel cell, since 700 °C is at the working limit for common metals [3]. Operation of SOFCs at low temperatures (LT-SOFC, 500–700 °C) may reduce material costs and sealing problems and thus is of great research interest [4]. However, the low conversion efficiencies of the steam reforming reaction at low temperatures lead to a drastic reduction in cell efficiency. An additional disadvantage of steam reforming is the large amount of steam that is needed to suppress carbon deposition when utilizing hydrocarbon fuels other than methane [5]. Moreover, it has been shown that even at high steam to carbon ratios (∼>3.5) in the case of internal reforming of ethane and ethylene, the power generation of SOFCs deteriorates with time due to carbon deposition [6]. Carbon deposition reduces the cell performance by blocking the anode reaction sites [7] and damaging the microstructure of Ni in the anode.

These disadvantages of internal reforming encourage current research attempts searching for a direct oxidation mechanism to utilize hydrocarbon fuels rather than internal reforming, with particular emphasis on development of coking resistant anode materials. Direct oxidation of hydrocarbon (HC) fuels may reduce the thermal gradients created by internal reforming and improve fuel conversion efficiency, particularly with heavier hydrocarbons than methane. However, when HC fuel is directly utilized on conventional nickel-based anodes, carbon deposited on the anode material due to a secondary cracking reaction blocks the reactants from reaching the reaction sites, degrades the nickel microstructure over time, and dramatically reduces the fuel cell performance and stability. Previous studies show that nickel can be utilized in direct oxidation of methane between 500 °C and 700 °C without carbon formation, but it is unlikely with higher hydrocarbons, since the temperature window for pyrolysis will be lower and carbon formation more severe [8]. This drives research attempts to find alternatives to the use of nickel in SOFC anodes for direct oxidation of hydrocarbon fuels.

In recent studies [9–12], copper has been suggested as an alternative to nickel as the electronic conductor in SOFC anodes. Copper has been used as the metal for inclusion in the anode due to its high electrical conductivity and relatively low catalytic activity for hydrocarbon cracking [9]. However, copper also has a low catalytic activity for hydrogen or hydrocarbon electrochemical oxidation, and so in order to improve the cell performance, ceria and samaria doped ceria (SDC) [10,11] have been utilized instead of yttria stabilized zirconia (YSZ), which is commonly used as the ionic conductor in SOFC anodes. The addition of a mixed conductor such as doped ceria has been shown to play an important role in improving anode performance, through improved catalytic activity and mixed ionic–electronic conductivity, which increases reaction surface area. Carbon deposition was not observed using this anode design. However, copper–SDC anodes tend to be unstable at high temperature due to the copper's relatively low melting temperature and high surface energy, resulting in rapid sintering of the copper and loss of electrode conductivity at temperatures above 800 °C [12].

Despite the advantages of copper-based anodes for direct oxidation, they are manufactured presently using a multi-step wet ceramic technique that requires even more processing and firing steps than needed to make nickel-based anodes by wet ceramic processing, which makes them less attractive for mass production.

SOFC processing typically includes a combination of wet powder compaction steps such as tape casting or extrusion, followed by deposition by a chemical or physical process such as spray pyrolysis, screen printing, or electrochemical vapor deposition, and then densification at elevated temperatures. The complex multi-step processing procedures are time consuming and require significant capital costs, particularly when scaled up for mass production. High sintering temperatures also increase the likelihood of interreactions between adjacent cell layers or of metal support oxidation in metallic interconnect-supported cells.

Recent studies (e.g. [9,10,12]) utilizing copper as the electronic conductor in SOFC anodes use impregnation of aqueous solutions of nitrate salts into a pre-sintered porous YSZ matrix. This procedure is used because the low melting temperature of copper oxide compared to that of nickel oxide prevents co-sintering of an anode layer containing copper oxide at a sufficiently high temperature to densify the YSZ electrolyte. This procedure adds further complexity to the wet ceramic manufacturing process, especially since multiple impregnation and firing steps are needed to obtain adequate connectivity of the anode metal phase.

1.2. Plasma spray processing for the production of SOFCs based on Cu–SDC anodes

Plasma spray processing has also been studied recently as a processing procedure for the manufacturing of SOFCs [13–17]. Plasma spraying has the advantages of short processing time, material composition flexibility, and a wide range of controllable spraying parameters that can be used to adjust the properties of the coatings. Controlling the spraying and feedstock parameters during spraying allows control of the coating characteristics, creating the opportunity to vary the coating properties with thickness to obtain a functionally graded material (FGM) structure that may lead to better electrochemical performance and reduced thermal stresses [16,17]. It also allows manufacturing of an entire cell in an integrated fabrication process [13], and spraying directly onto robust metallic interconnects, thus lowering material costs, with no requirement for sintering [14]. Nano-structured anodes have also been produced by plasma spraying of nano-agglomerated feedstock powder [18]. This approach can provide more triple phase boundaries for the hydrogen oxidation reaction and contribute to lowering polarization losses. Plasma spray processing can also be scaled up easily for rapid, automated mass production, which may allow further reduction of manufacturing costs.

To date, plasma sprayed Cu–SDC anode testing in a working cell has not previously been reported. The primary challenge in making such anodes by plasma spraying is the large difference between the melting temperature of CuO and SDC (1326 °C for copper oxide and 2600 °C for SDC), which makes it difficult to co-deposit these materials. Co-deposition of materials with a large melting temperature difference, such as tungsten carbide–cobalt coatings, has been conducted previously by plasma spraying [19]. However, that application does not require coatings with significant porosity, so both materials can be co-deposited in a high-energy plasma that fully melts both materials, resulting in dense coatings. However, the requirement for high porosity of SOFC anodes for good diffusivity makes it more difficult to co-deposit materials with a large difference between the melting temperatures in a coating having a porous structure. It is advantageous to co-spray CuO and SDC rather than Cu and SDC due to the higher melting temperature of CuO (1326 °C) and because the reduction of CuO to Cu after cell fabrication results in additional porosity.

It has been shown [20] that the addition of more catalytically active materials such as cobalt to Cu–SDC anodes is beneficial.

Nevertheless, due to the higher cost of cobalt, direct oxidation anodes are likely to contain at least a portion of their structure consisting entirely of Cu–ceramic mixtures, to function primarily as a current collector/gas diffusion layer within the anode. Therefore, coarse layers containing only Cu and SDC are still of practical importance for application in direct oxidation SOFC anodes.

Cu–SDC anodes exhibit lower catalytic activity compared to conventional Ni–YSZ anodes due to the set of materials utilized in such anodes. Therefore, increased triple phase boundary surface area in an anode functional layer is important in improving anode performance. This study utilizes nano-agglomerated powders for the production of nano-structured plasma sprayed Cu–SDC coatings for use in an anode functional layer to achieve higher surface area and improved performance relative to coarser diffusion layers.

Previously, Cu–YSZ layers have been sprayed onto stainless steel coupons [21]. However, these layers have not been tested as anodes in a working cell. In addition, it is more beneficial to replace the YSZ with ceria or SDC, as ceria or SDC enhances the catalytic activity in Cu-based anodes [9]. CuO–SDC layers have also been sprayed onto ceramic substrates and the CuO has been successfully reduced to copper in hydrogen [22]; however, the layers were not tested as anodes in electrochemical cells.

We have recently applied plasma spray processing for the manufacturing of metal supported fuel cells with Cu–SDC ($Ce_{0.8}Sm_{0.2}O_{1.9}$) SOFC anode layers utilizing nano-agglomerated feedstock powders. In this article, we present the spraying and feedstock conditions developed and used to co-deposit CuO–SDC SOFC anode layers, their resulting elemental and phase compositions, their microstructures before and after reduction of CuO to Cu, and their electrochemical performance in a solid oxide fuel cell.

2. Experimental procedure

2.1. Material preparation

In this work, commercially available feedstock powders of CuO and SDC ($Ce_{0.8}Sm_{0.2}O_{1.9}$) (Inframat Advanced Materials, Farmington, CT, USA) were used to fabricate the coatings. The powders were flowable spray dried agglomerates with a spherical shape. Two different powders were used in this study: coarse and fine powders. Coarse powders were utilized for the initial screening tests and for the production of symmetrical cells. Fine powders were utilized to produce anode layers on porous metal-supported cells. Particle size analysis was conducted using a wet dispersion laser light scatting particle size analyzer (Mastersizer 2000, Malvern Instruments, Worcestershire, UK). Table 1 shows the powder particle size distributions. Fig. 1 shows scanning electron microscopy (SEM) images of the spray dried nano-agglomerated CuO and SDC feedstock powders.

Table 1
Particle sizes of coarse and fine powders.

Powder	Coarse (μm)		Fine (μm)	
	CuO	SDC	CuO	SDC
$D_{0.1}$	4.33	23.3	2.41	1.80
$D_{0.5}$	12.9	36.7	8.29	2.50
$D_{0.9}$	36.1	58.0	20.10	13.2

For the initial screening tests, the as-received coarse CuO and SDC powders were sieved to narrower size distributions of +32–45 μm. The powders were mixed with a weight ratio of 1:1.2 SDC to CuO.

For spraying of Cu–SDC anodes for electrolyte supported symmetrical cells, we utilized smaller CuO particles sieved to −25 μm to allow more fine scale mixing of the CuO splats with the SDC in the coating. The CuO and SDC powders were mixed in those coatings with a weight ratio of 1:1.5 SDC to CuO.

For spraying of Cu–SDC anodes for porous metal-supported full cells, the fine CuO and SDC powders were utilized to produce a microstructure with higher triple boundary length to improve performance. The CuO and SDC powders were mixed in those anodes with a weight ratio of 1:1.67 SDC to CuO

2.2. Plasma spray processing

The atmospheric plasma spray (APS) system used in these experiments (Axial III Series 600 DC plasma torch, Northwest Mettech Corp., North Vancouver, Canada) contains a torch in which powder is injected axially between three electrodes, ensuring that virtually all of the powder injected passes through the hottest part of the jet. Powders were delivered to the torch with Ar carrier gas using powder feeders (MPF Thermico, Dortmund, Germany). The APS system further consisted of a substrate-mounting turntable for both generating horizontal substrate motion relative to the torch and for the cooling of the substrates in air. A type 'K' thermocouple was spring loaded to the back of the substrate, with the signal carried from the rotating substrate holder through a slip ring to allow substrate temperature monitoring. An X–Y manipulator (Miller Thermal Inc, Appleton, WI, USA) was used to move the plasma torch vertically. Fig. 2 schematically depicts the APS experimental setup.

Preliminary screening tests were carried out with mixed CuO and SDC powders. The plasma gas composition was changed for each of the coatings. Deposition was carried out onto sandblasted 2.54 cm diameter 1 mm thick type 430 stainless steel (SS430) disks.

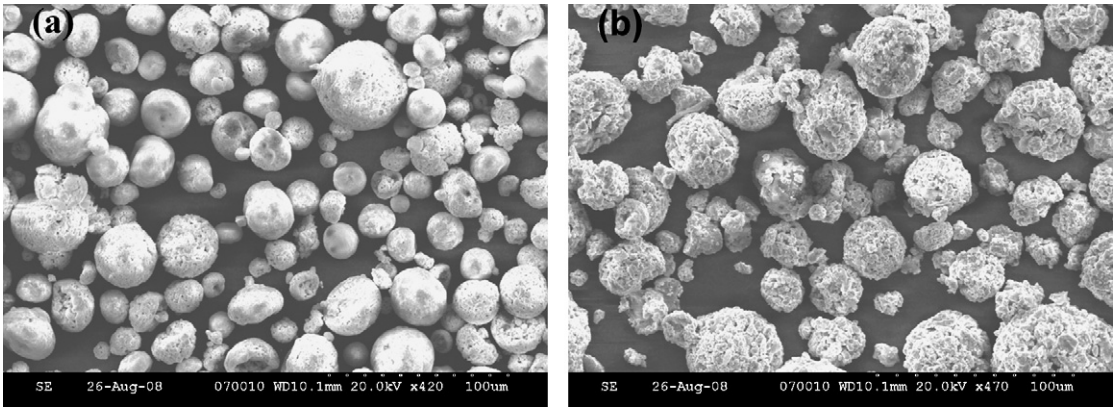

Fig. 1. SEM micrographs of (a) SDC and (b) CuO.

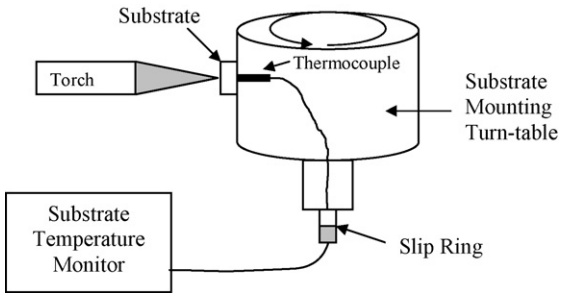

Fig. 2. APS experimental setup.

The coatings were reduced after deposition in a 90:10 vol.% N_2–H_2 mixture at 700 °C for 12 h.

Following the identification of the usable range of plasma gas composition values, symmetrical cells were produced. YSZ powder (Inframat Advanced Materials, d_{50} = 1.58 μm) was pressed into pellets with a 32 mm die. The pellets were sintered at 1400 °C for 4 h. The sintered YSZ substrates were sand blasted prior to spraying to create a coarse surface in order to allow better adhesion of the coating to the surface. After sand blasting, the surfaces were cleaned with acetone to remove any residue. The anode layer coatings were deposited symmetrically on both sides of the substrates, using a custom made mask to obtain concentric anodes. To obtain full percolation in porous composite anodes, the volume fraction of the Cu in the solid phases of the anode was targeted at 40%, in keeping with the observed upper percolation threshold range for Ni–YSZ anodes [23]. The symmetrical cell anode layer coatings produced were reduced in H_2 at 700 °C for 5 h.

Due to the performance and mechanical limitations introduced by electrolyte-supported cells, we then integrated porous metallic substrates into subsequent cells as a substitute for the YSZ electrolyte supports. Commercially available 2.54 cm diameter porous SS430 disks (Mott Corporation, Farmington, CT, USA) with thickness of 1 mm were used as the metallic substrates. One such substrate is shown in Fig. 3.

SS430 was chosen due to its low thermal expansion coefficient (11.9 μm m^{-1} °C^{-1} at 650 °C), which allows a better thermal expansion match between the substrate and the cathode–electrolyte–anode layers than Ni, which has been previously utilized as the substrate material [24]. A cathode layer was formed by spraying mechanically mixed LSM-YSZ powders (Inframat Advanced Materials) onto the substrate using conditions developed previously [25]. Fine YSZ powder (Inframat Advanced Materials) suspended in water was used to form the electrolyte on top of the cathode using conditions reported elsewhere [26]. CuO and SDC powders were mixed with a weight ratio of 1:1.67 SDC to CuO. This powder mixture was sprayed through a mask onto the YSZ layer to form an anode layer. The coatings were reduced after deposition in a N_2–H_2 mixture (10% H_2) at 700 °C for 12 h. Table 2 shows experimental plasma spray process parameters for anode production for the different tests.

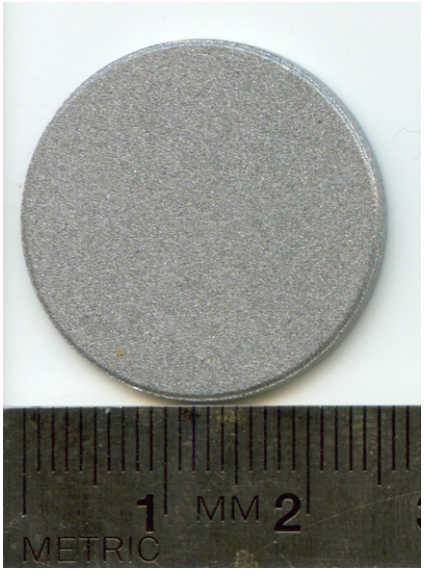

Fig. 3. Porous SS430 metal substrate.

2.3. Coating characterization

X-ray diffraction (XRD) analysis of the coatings was performed both before and after reduction to determine the phase structure dependence on spraying and feedstock parameters.

SEM imaging of the coatings was performed to observe the porosity and uniformity of the microstructures.

Energy dispersive spectroscopy (EDX) was performed to determine the volume fraction of Cu present in the coatings.

2.4. Electrochemical testing

Symmetrical cell testing was performed using an SOFC test station (AMI, Canada, and AMEL, Italy) and an FRA and potentiostat (Solartron 1260 and 1470E, UK) after in situ reduction in H_2 at 569 °C of the anodes. The test station design includes a thermocouple that measures the temperature close to the cell. The symmetrical cell was tested in dry hydrogen flowing at 100 sccm at temperatures ranging from 569 °C to 772 °C, in approximately 50 °C increments with 3 °C min^{-1} ramp rates between temperatures. Impedance spectroscopy at open circuit conditions was

Table 2
Plasma spray process parameter values for production of anode coatings.

Parameter	Values		
	Initial screening tests	Symmetrical anode–anode cell experiments	Metal substrate full cell experiments
Powder feed rate (g min^{-1})	32	18	40
Carrier gas flow rate (slpm]	15	15	15
Spraying distance (mm)	100	100	100
SDC particle size (μm)	−45 + 32	−32 + 25	2.5 (d_{50})
CuO particle size (μm)	−45 + 32	−25	8.2 (d_{50})
Weight ratio SDC/CuO	1.2	1.5	1.67
Vertical traverse speed (m s^{-1})	4.25	4.25	4.25
No. of vertical passes	40	40	40
Torch current (A $electrode^{-1}$)	200	180	200
Plasma gas flow rate (slpm)	220	180	220
Vol.% nitrogen (balance Ar)	20–80	50	40
Nozzle size (mm)	12.7	12.7	12.7

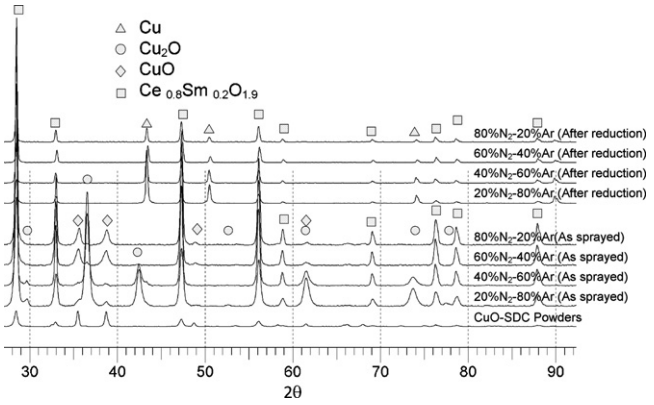

Fig. 4. XRD patterns of coatings produced from CuO–SDC feedstock powders over various plasma gas compositions. *Y*-axis represents X-ray intensity in arbitrary units.

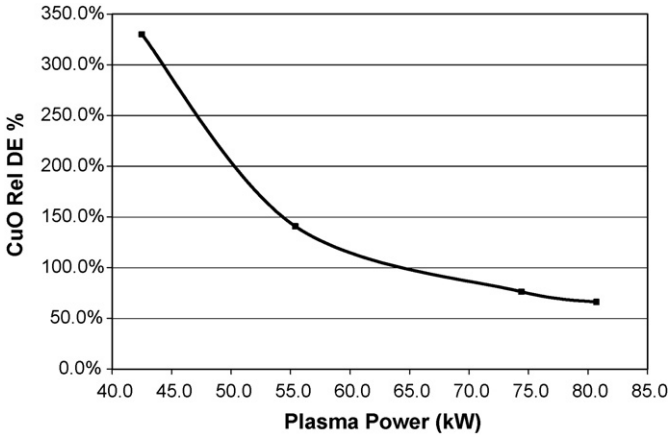

Fig. 5. CuO deposition efficiency relative to that of SDC with varying plasma power.

conducted at cell temperatures of 569 °C, 620 °C, 672 °C, 723 °C, and 772 °C over the frequency range of 2 mHz to 1 MHz, with 50 mV rms voltage perturbation amplitude.

The CuO–SDC anodes in full cells were reduced in situ with a humid (3% H_2O) H_2–N_2 mixture (10% H_2) at a total flow rate of 100 sccm for 13 h at 700 °C. The cells were then tested in a humid (3% H_2O) H_2–N_2 mixture (20% H_2) at a total flow rate of 0.2 slpm at temperatures ranging from 550 °C to 700 °C, in approximately 50 °C increments with 1 °C min^{-1} ramp rates between temperatures. Impedance spectroscopy at open circuit voltage (OCV) and at 0.7 V polarization was conducted at cell temperatures of 562 °C, 612 °C, 672 °C, and 712 °C over the frequency range of 1 mHz to 1 MHz, with 50 mV rms voltage perturbation amplitude. Polarization curves were obtained from OCV to 0.3 V.

After testing with H_2, the cells were exposed to CH_4 for 12 h. After the cells were cooled down, they were examined by EDX to search for carbon residue.

3. Results and discussion

3.1. Microstructural analysis

3.1.1. Microstructural analysis of screening test coatings

XRD showed that the crystal structure of the SDC remained cubic over the entire range of spraying conditions. In high-energy plasmas with plasma gas composition of N_2–Ar 60–40% and 80–20% by volume, the CuO remained cubic. For lower energy plasmas with plasma gas composition of N_2–Ar 40–60% and 20–80%, partial reduction of CuO to Cu_2O was observed. XRD patterns of the coatings after reduction in a 10–90% H_2–N_2 mixture confirmed that the CuO and Cu_2O were fully reduced to Cu. Fig. 4 shows XRD patterns of coatings produced from CuO–SDC feedstock powders, before and after reduction.

The main difficulty in producing CuO/SDC composite anode coatings by APS is achieving the desired composition, 40 vol.% of Cu, due to the differences in deposition efficiency between the two materials for a given set of plasma conditions, as shown in Fig. 5. Therefore, once suitable spray conditions were determined, the initial powder compositions were adjusted based on the EDX results in order to obtain a composition close to the target range.

Fig. 6 shows SEM micrographs of coatings produced in different plasma energy conditions. Over the spraying conditions examined, the CuO tends to melt easily to form thin, fairly dense layers within the coating. Fig. 6a shows a coating formed in a high-power (80.7 kW) plasma. The CuO phase is well melted and forms splats that spread over the less melted SDC particles. Fig. 6b shows a coating formed in a lower-power plasma (55.4 kW). It can be seen that the CuO is very highly melted, even in the lower-power plasma. It can also be seen that the spray dried SDC agglomerates break up into smaller particles during the spraying process. This is likely a result of a combination of low particle temperature and high particle velocity at the time of impact with the substrate. EDX mapping showed that although the CuO and SDC in the coatings are well mixed on the mm scale, the coatings are not homogenous and the SDC and CuO are not well mixed on the μm scale. It is not clear whether the SDC agglomerates break up upon entering the plasma

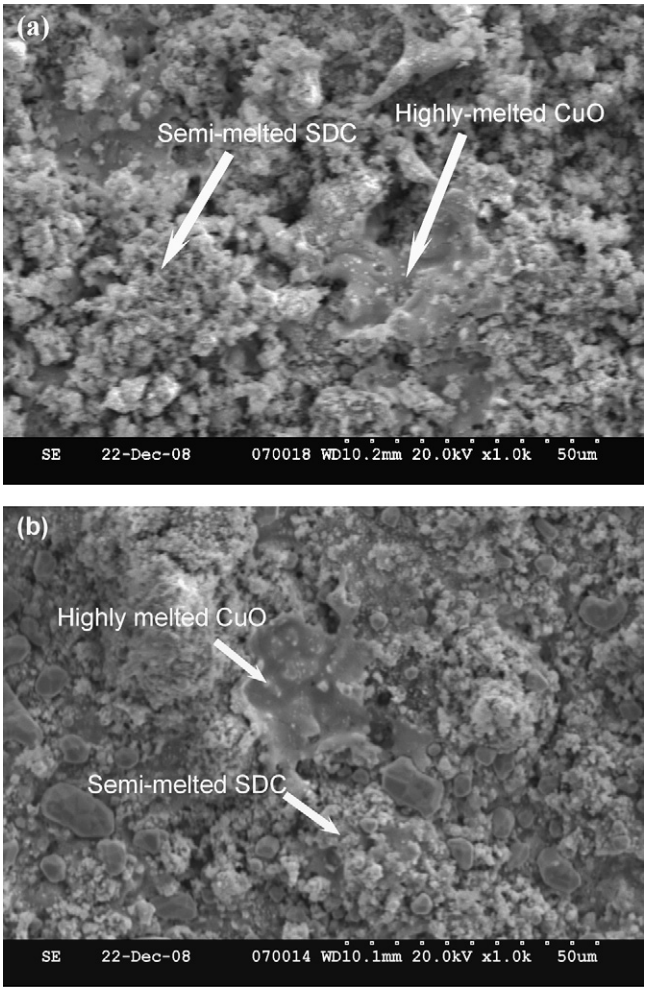

Fig. 6. APS CuO–SDC coatings sprayed with (a) high (80.7 kW) and (b) low (55.4 kW) plasma energy conditions.

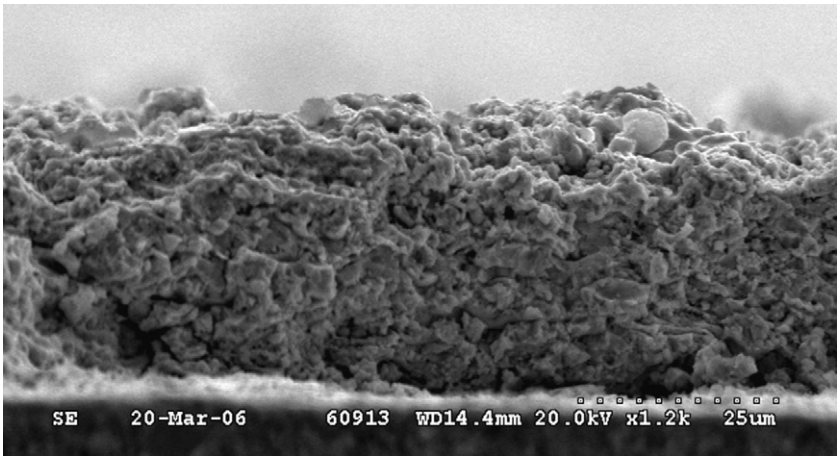

Fig. 7. Cross-section of an anode coating produced for a symmetrical cell with the set of spraying parameters and conditions shown in Table 2.

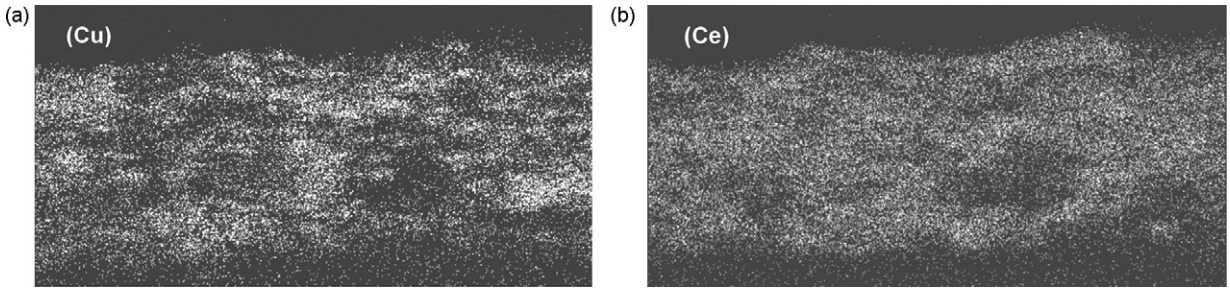

Fig. 8. EDX maps of a Cu–SDC coating produced for a symmetrical cell with the set of spraying parameters and conditions shown in Table 2.

or whether the droplets only partially melt in the plasma, leading to breaking up of the particles upon impact with the substrate, but clusters of SDC remain intact in the coatings. The SDC particles in the coating show a wide size distribution, from sub-micron to tens of microns.

3.1.2. Symmetrical cell microstructural analysis

After analyzing the results from the screening tests, further modifications were made to the spraying and feedstock conditions. The CuO particle size was decreased to reduce the size of the splats of the highly melted CuO particles and to improve the extent of mixing with the SDC to improve the microstructure. The SDC particle size was decreased to allow the coatings to be sprayed with a lower plasma power in order to produce coatings on YSZ substrates without breaking them due to thermal shock and to increase the surface area for reaction. The plasma gas flow rate was reduced to allow higher residence times of the particles in the plasma and therefore better melting of the SDC particles.

Fig. 7 shows a cross-section SEM micrograph of a coating produced with the set of spraying parameters and conditions listed in Table 2 for symmetrical cells, after reduction with H_2. It can be seen that decreasing the SDC and CuO particle sizes and applying a low plasma gas flow rate resulted in coatings with a more uniform, porous, and well mixed microstructure with the desired characteristics of anodes: fairly high surface area, porosity, and extensive CuO–SDC mixing and contact. Fig. 8 shows EDX maps of the coating, confirming that the CuO and SDC phases are fairly well mixed. EDX measurements determined that the volume fraction of Cu in the coatings after reduction was 39.8 vol.%.

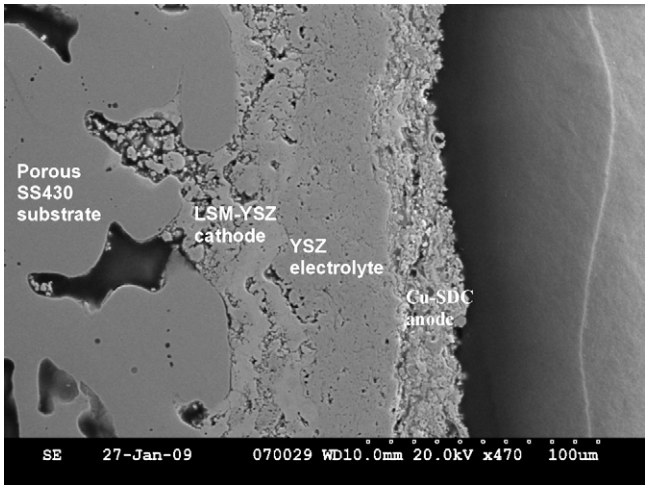

Fig. 9. Cross-section of metal-supported cell.

3.1.3. Metal-supported cell microstructural analysis

Fig. 9 shows an SEM micrograph of a metal supported cell cross-section. As seen in the SEM micrograph, the anode is porous, with a thickness of approximately 20 μm. The use of fine SDC and CuO particles resulted in a fine microstructure with fairly high surface area. An EDX map of the anode is shown in Fig. 10. From the map, it can clearly be seen that the Cu and SDC phases are well mixed. EDX measurements determined that the volume fraction of Cu in the coatings after reduction was 35 vol.%. EDX of the cell after testing in methane revealed no carbon residue on the anode surface.

3.2. Electrochemical performance

3.2.1. Symmetrical cell electrochemical performance

Impedance spectroscopy was conducted on an electrolyte supported Cu–SDC double-anode symmetrical cell over the temper-

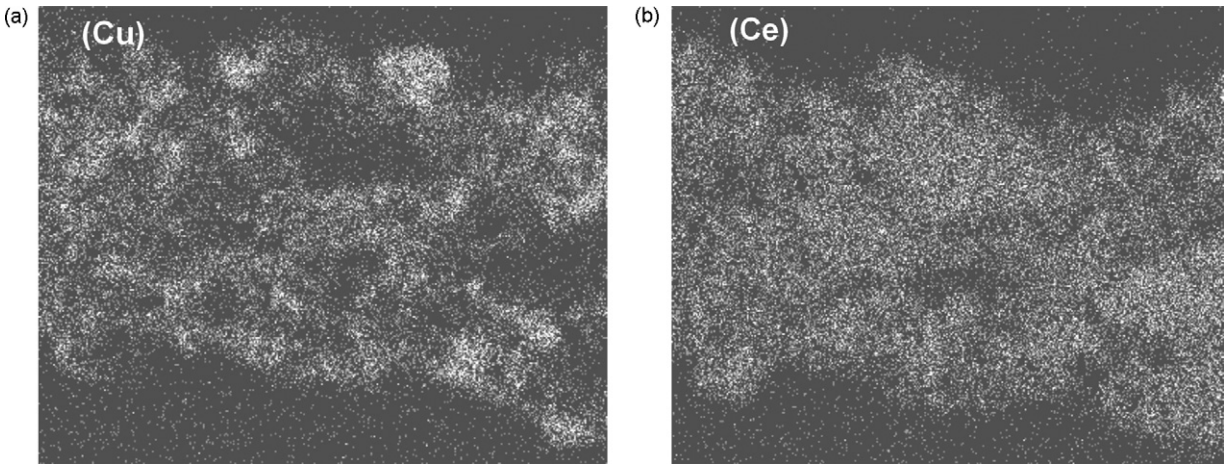

Fig. 10. EDX map of a Cu–SDC anode layer in a metal-supported cell.

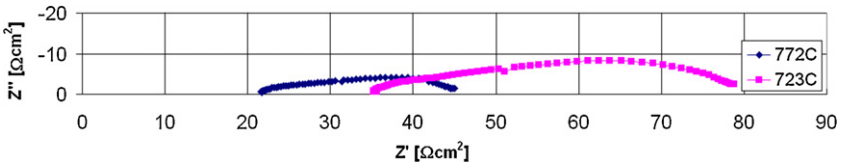

Fig. 11. Impedance spectra of an electrolyte-supported symmetrical cell at OCV.

ature range from 620 °C to 772 °C. The measurements were repeated several times during 90-min holds at each temperature. Fig. 11 shows the impedance spectra of the symmetrical cell at 723 °C and 772 °C. Each impedance spectrum shown was obtained after 30 min of dwelling at the specific temperature. Impedance values are normalized to electrode area.

The area-specific polarization resistance for each anode is shown in Table 3 for all temperatures tested, assuming that each anode in the symmetrical cell has the same polarization resistance. The fairly high area-specific polarization resistance is at least in part due to the extremely low catalytic activity of the Cu in the anode layer, and partly due to the need for further microstructural refinement.

3.2.2. *Metal-supported cell electrochemical performance*

Polarization curves of the metal-supported cell at temperatures from 600 °C to 700 °C are shown in Fig. 12. Nyquist impedance plots at cell polarizations of 0.7 V and OCV can be seen in Fig. 13. Corresponding Arrhenius plots of the cell polarization resistances determined from the EIS testing of the metal-supported cell at OCV are shown in Fig. 14, along with results from cathode–cathode symmetrical cell testing reported in the literature using the same cathode processing parameters [25]. Arrhenius plots of the anode–anode symmetrical cell testing results are also shown in Fig. 14, along with calculated values of ASR_p from the metal-supported cell tests, calculated from the full cell impedance values at OCV and the symmetrical cell cathode ASR_p values. Activation energies for the four configurations were found to be 0.90 eV for the anode–anode symmetrical cell, 0.91 eV for the cathode–cathode symmetrical cell, 0.69 eV for the calculated anode ASR_p in a metal-supported cell, and 0.72 eV for the metal-supported full cell. An Arrhenius plot of the metal supported cell ohmic resistance is also shown in Fig. 14. The activation energy of the ohmic resistance of the metal-supported cell was found to be 1.0 eV. This value is similar to values reported in the literature for APS electrolytes [27]. Table 3 shows the polarization resistances obtained by EIS testing of the metal-supported cell and the corresponding cathodic polarization resistance [25], anodic polarization resistance from electrolyte-supported symmetrical cells, and anodic polarization resistance calculated for the anodes in the metal-supported full cells.

Table 3
Summary of area-specific polarization resistances of a metal-supported cell and of a symmetrical electrolyte-supported cell.

ASR_p ($\Omega\,cm^2$) at OCV					
Metal-supported cell				Electrolyte-supported cell	
T (°C)	Full cell	Cathode	Calculated anode	T (°C)	Anode
712	5.51	0.73	4.78	772	12.4
660	10.9	1.34	9.55	723	21.8
610	15.9	2.55	13.4	672	38.5
560	27.6	5.26	22.3	620	67.4

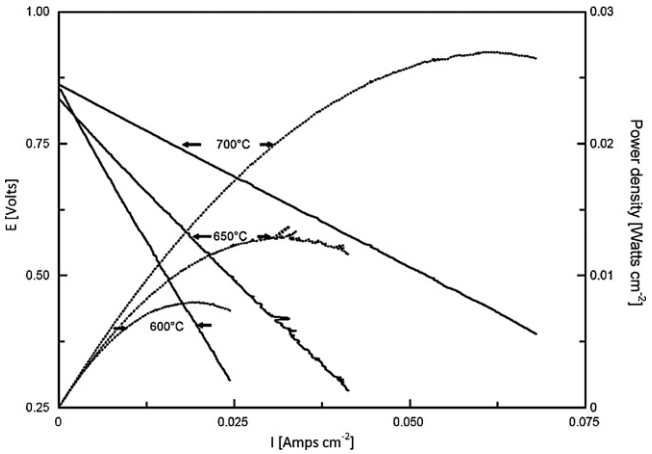

Fig. 12. Polarization curves of a metal-supported cell.

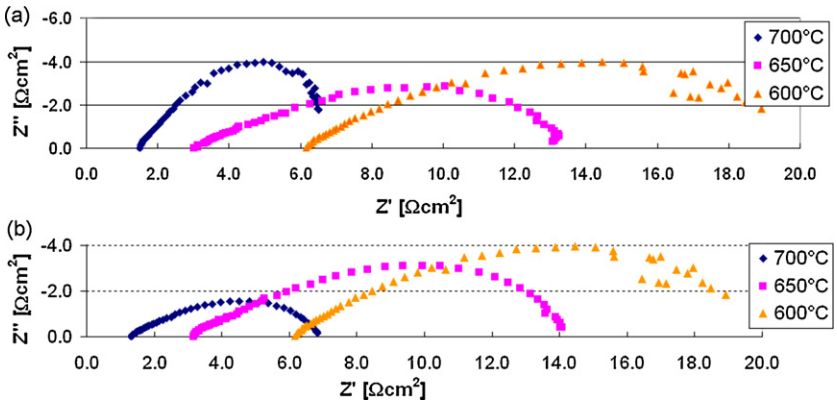

Fig. 13. Nyquist plots at cell polarizations of (a) 0.7 V and (b) OCV at various temperatures.

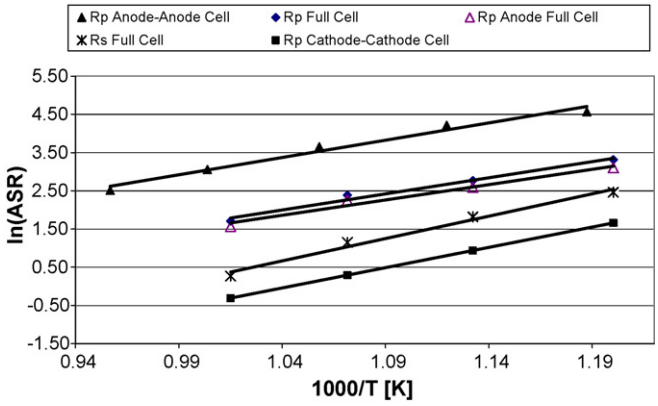

Fig. 14. Arrhenuis plots of the metal-supported cell, metal-supported cathode–cathode symmetrical cell [25], and electrolyte-supported anode–anode symmetrical cell. ASR given in units of $\Omega\,cm^2$.

4. Conclusions

Cu–SDC anode coatings have been fabricated and tested in electrolyte-supported symmetrical cell and full metal-supported cell configurations. CuO and SDC powders were sprayed simultaneously onto electrolyte supports or electrolyte coatings on metal-supported cathodes and subsequently reduced in hydrogen to produce Cu–SDC anode layers on test substrates, electrolyte supported symmetrical cells, and metal-supported full cells. Using fine powder feedstock and the spraying conditions developed, well mixed coatings with 35–40 vol.% Cu were fabricated, and a calculated anode polarization resistance of 4.78 $\Omega\,cm^2$ was obtained with the Cu–SDC anodes at 712 °C in metal-supported cell tests. Additional improvements can likely be achieved through the addition of Co or other more catalytically active materials; these studies are currently underway.

Acknowledgements

The authors gratefully acknowledge the generous support of Northwest Mettech Corp. and the Natural Sciences and Engineering Research Council of Canada for funding and of the National Research Council Institute for Fuel Cell Innovation (NRC-IFCI) for access to their facilities. This research was supported in part through funding to the NSERC Solid Oxide Fuel Cell Canada Strategic Research Network from the Natural Science and Engineering Research Council (NSERC) and other sponsors listed at www.sofccanada.com. The authors gratefully acknowledge the assistance of Mr. David Waldbillig for the production of suspension sprayed electrolytes for the full cells, and the generous help of Dr. Cyrille Deces-Petit from NRC-IFCI for the testing of symmetrical cells and the design and maintenance of testing equipment.

References

[1] J. Larminie, A. Dicks, Fuel Cells Systems Explained, Wiley Chichester, 2000, pp. 192–193.
[2] R. Peters, R. Dahl, U. Klüttgen, C. Palm, D. Stolten, J. Power Sources 106 (2002) 238–244.
[3] R.J. Gorte, S. Park, J.M. Vohs, C. Wang, Adv. Mater. 12 (19) (2000) 1465–1469.
[4] J. Molenda, K. Swierczek, W. Zajac, J. Power Sources 173 (2007) 657–670.
[5] S. Mclntosh, R.J. Gorte, Chem. Rev. 104 (2004) 4845–4865.
[6] K. Eguchi, H. Kojo, T. Takeguchi, R. Kikuchi, K. Sasaki, Solid State Ionics 152–153 (2002) 411–416.
[7] J. Maček, B. Novosel, M. Marinšek, J. Eur. Ceram. Soc. 27 (2007) 487–491.
[8] S. Park, R.J. Gorte, J.M. Vohs, Appl. Catal. A: Gen. 200 (2000) 55–61.
[9] R.J. Gorte, H. Kim, J.M. Vohs, J. Power Sources 106 (2002) 10–15.
[10] C. Lu, W.L. Worrell, J.M. Vohs, R.J. Gorte, J. Electrochem. Soc. 150 (10) (2003) A1357–A1359.
[11] S. Zhao, R.J. Gorte, Appl. Catal. A: Gen. 277 (2004) 129–136.
[12] M.D. Gross, J.M. Vohs, R.J. Gorte, J. Mater. Chem. 17 (2007) 3071–3077.
[13] X.Q. Ma, H. Zhang, J. Dai, J. Roth, R. Hui, T.D. Xiao, D.E. Reisner, J. Therm. Spray Technol. 14 (1) (2005) 61–66.
[14] G. Schiller, R. Henne, M. Lang, M. Muller, Fuel Cell 4 (1–2) (2004) 56–61.
[15] S. Kim, O. Kwon, S. Kumar, Y. Xiong, C. Lee, Surf. Coat. Technol. 202 (2008) 3180–3186.
[16] R. Hui, Z. Wang, O. Kesler, L. Rose, J. Jankovic, S. Yick, R. Maric, D. Ghosh, J. Power Sources 170 (2007) 308–323.
[17] R. Henne, J. Therm. Spray Technol. 16 (3) (2007) 381–403.
[18] C. Hwang, C. Yu, Surf. Coat. Technol. 201 (12) (2007) 5954–5959.
[19] J. Iwaszko, Z. Nitkiewicz, Mater. Manuf. Process. 17 (2) (2002) 169–176.
[20] S. Lee, J.M. Vohs, R.J. Gorte, J. Electrochem. Soc. 151 (9) (2004) A1319–A1323.
[21] A. Benyoucef, D. Klein, C. Coddet, B. Benyoucef, Surf. Coat. Technol. 202 (2008) 2202–2207.
[22] N. Ben-Oved, O. Kesler, Adv. Mater. Res. vols. 15–17 (2007) 287–292.
[23] J.H. Lee, H. Moon, H.-W. Lee, J. Kim, J.-D. Kim, K.-H. Yoon, Solid State Ionics 148 (2002) 15–26.
[24] M. Lang, T. Franco, G. Schiller, N. Wagner, J. Appl. Electrochem. 32 (2002) 871–874.
[25] B.D. White, O. Kesler, L. Rose, J. Power Sources 178 (2008) 334–343.
[26] D. Waldbillig, O. Kesler, Surf. Coat. Technol. 203 (2009) 2098–2101.
[27] Zhang, C.-J. Li, G. Zhang, X.-J. Ning, C.-X. Li, H. Liao, C. Coddet, Mater. Sci. Eng. B 137 (2007) 24–30.